Magnetic proximity effect in Nb/Gd superlattices seen by neutron reflectometry

Yu. N. Khaydukov,[1,2,3] E. A. Kravtsov,[4,5] V. D. Zhaketov,[6] V. V. Progliado,[4] G. Kim,[1] Yu. V. Nikitenko,[6]
T. Keller,[1,2] V. V. Ustinov,[4,5] V. L. Aksenov,[6] and B. Keimer[1]

[1]*Max-Planck-Institut für Festkörperforschung, Heisenbergstraße 1, D-70569 Stuttgart, Germany*
[2]*Max Planck Society Outstation at the Heinz Maier-Leibnitz Zentrum (MLZ), D-85748 Garching, Germany*
[3]*Skobeltsyn Institute of Nuclear Physics, Moscow State University, Moscow 119991, Russia*
[4]*Institute of Metal Physics, Ekaterinburg 620180, Russia*
[5]*Ural Federal University, Ekaterinburg 620002, Russia*
[6]*Joint Institute for Nuclear Research, Dubna 141980, Russia*

We have used spin-polarized neutron reflectometry to investigate the magnetization profile of superlattices composed of ferromagnetic Gd and superconducting Nb layers. We have observed a partial suppression of ferromagnetic (F) order of Gd layers in $[Gd(d_F)/Nb(25 \text{ nm})]_{12}$ superlattices below the superconducting (S) transition of the Nb layers. The amplitude of the suppression decreases with increasing d_F. By analyzing the neutron spin asymmetry we conclude that the observed effect has an electromagnetic origin—the proximity-coupled S layers screen out the external magnetic field and thus suppress the F response of the Gd layers inside the structure. Our investigation demonstrates the considerable influence of electromagnetic effects on the magnetic properties of S/F systems.

Artificial heterostructures with alternating superconducting (S) and ferromagnetic (F) layers are currently attracting great attention due to a diverse set of proximity effects [1–5], including the Larkin-Ovchinnikov-Fulde-Ferrell phase, π-phase superconductivity, and triplet pairing. These effects show how ferromagnetism influences the superconducting properties of the S/F heterostructures. Converse proximity effects in which superconductivity influences ferromagnetism have received less attention. Such magnetic proximity effects are expected in systems where the F and S transition temperatures, T_F and T_c, are comparable, which is the case for heterostructures of cuprate high-T_c superconductors and ferromagnetic manganates [6–9], and for some bulk compounds [10–12]. However, because of the chemical and electronic complexity of these materials, simple model systems for magnetic proximity effects are highly desirable.

For most S/F heterostructures composed of elemental metals or alloys, T_F greatly exceeds T_c. In such systems, one still expects significant magnetic proximity effects if the effective energy $E_F \sim T_F d_F/d_S$ becomes comparable to $E_S \sim T_c$, where d_F (d_S) are the thicknesses of the F (S) layers [1]. The first to indicate such a possibility were Anderson and Suhl [13]. They considered systems consisting of S and F phases and came to the conclusion that a homogeneous magnetic phase above T_c may become inhomogeneous below T_c. Such a transition, which they called cryptoferromagnetism (CFM), would depress the effective exchange field of ferromagnetism, thus enabling the coexistence of superconductivity and magnetism. Later on, the concept of CFM was further investigated in the theoretical work of Buzdin and Bulaevsky [14] and Bergeret *et al.* [15]. Recently, Zhu *et al.* reported the observation of an increased coercivity below T_c in GdN/Nb/GdN trilayers [16]. The authors interpreted this

increase as a superconductivity-driven antiferromagnetic (AF) alignment of the GdN layers.

The ability to control the magnetic state by superconductivity is attracting attention also in applied research on superconducting spintronics [17,18] including such new approaches as neuromorphic computing [19–21]. At the moment, most research efforts are focused on simple S/F structures such as bilayers and trilayers [22–24]. However, both the superconducting and the magnetic properties of more complex S/F systems, such as $[S/F]_n$ superlattices, may qualitatively differ from the properties of their S/F unit cells, thus opening up perspectives for novel functionalities. An essential difference in behavior is expected when the thickness of the S and/or F layer becomes comparable to the respective superconducting coherence length which specifies the strength of the superconducting correlations in the S (ξ_S) or F (ξ_F) layers [25–29]. The preparation of such superlattices requires a proper choice of materials with thin F and S layers and uniformity of the layer characteristics throughout the entire structure. Moreover, the S and F materials should be chosen in such a way as to increase the transparency of the S/F interface, that is, the leakage rate of superconducting correlations into the F layer(s).

Our recent study of Nb(25 nm)/Gd(d_F)/Nb(25 nm) trilayers has shown that high-quality structures with highly transparent S/F interfaces and rather high coherence length $\xi_F = 4$ nm can be grown [30]. Moreover, gadolinium is a weak ferromagnet with $T_F = 293$ K, which, in combination with Nb, the strongest elemental superconductor with $T_c = 9.3$ K, allows for the preparation of S/F systems with $E_F \sim E_S$. In this Rapid Communication, we report on a study of the magnetic and superconducting properties of superlattices of composition $[Gd(d_F)/Nb(25 \text{ nm})]_{12}$. The superlattices were deposited on 25×25 mm^2 $(1\bar{1}02)$Al$_2$O$_3$ substrates and
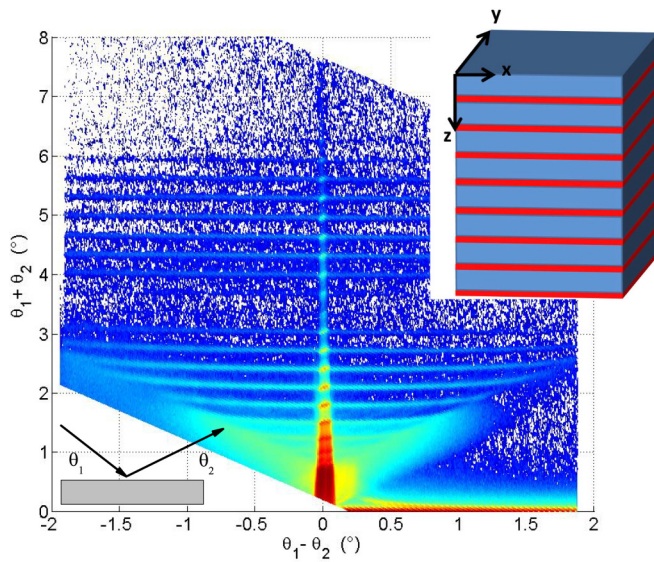
FIG. 1. X-ray scattering map of sample 2. The bottom inset shows the scheme of the reflectometric experiment. The upper inset shows a sketch of the structure where blue and red colors indicate Nb and Gd layers, respectively.

covered by a Nb(5 nm) capping layer. Later on, we cut $\sim 5 \times 5$ mm^2 pieces for magnetization and transport measurements (details of the sample preparation can be found in Ref. [30]). The thickness of the Gd layers was chosen to be $d_F = 0.5\xi_F$ (sample 1), $0.75\xi_F$ (sample 2), and $1.25\xi_F$ (sample 3). Figure 1 shows an x-ray scattering map measured on sample 2 at the NREX neutron/x-ray reflectometer (details can be found in Ref. [31]). The specular channel $\theta_2 = \theta_1$ exhibits more than 15 Bragg peaks arising from diffraction on the superlattice with period $D = d_F + d_S$, demonstrating high repeatability of a Gd/Nb bilayer in the z direction. In addition, we have detected diffuse scattering for $\theta_2 \neq \theta_1$ in the form of tilted lines around the specular Bragg peaks. These Bragg-like sheets indicate a high statistical correlation of the in-plane roughness profiles of Nb/Gd interfaces in the periodic structure [32].
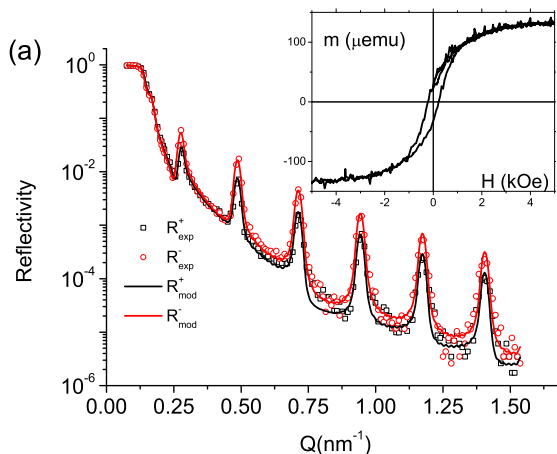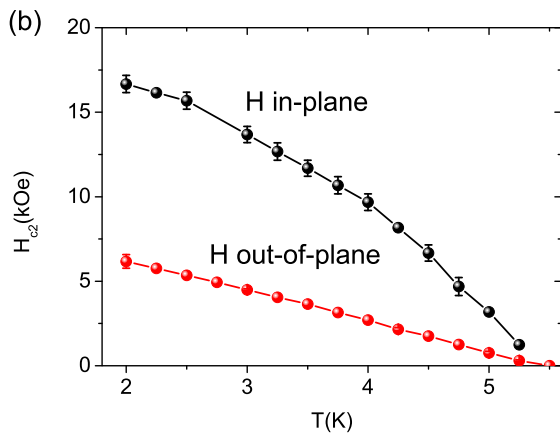
To study the magnetic properties of our superlattices we used polarized neutron reflectometry (PNR), which has been widely used for the study of S/F systems [6–9,33–36]. PNR allows measurements of the depth profile of the in-plane magnetization with nanometer depth resolution. Figure 2(a) shows typical spin-up R^+ and spin-down R^- reflectivity curves measured on sample 1 at $T = 7$ K (that is, in the normal state above T_c) and $H = 4.5$ kOe after cooling the sample in the same field. The neutron reflectivity exhibits six Bragg peaks positioned at $Q_n \approx 2\pi n/D$. The difference of R^+ and R^- clearly indicates the presence of an in-plane magnetic moment. Using the Born approximation, one can show that the spin asymmetry at the nth Bragg peak $S_n \equiv [R^+(Q_n) - R^-(Q_n)]/[R^+(Q_n) + R^-(Q_n)]$ is proportional to the magnetic contrast $M_{Gd} - M_{Nb}$ of a unit cell, where $M_{Gd,Nb}$ is the in-plane magnetization of a Gd and Nb layer, respectively. In the first approximation we may neglect the small magnetization of the Nb layers ($M_{Gd} \gg M_{Nb}$) and write $S_n \sim M_{Gd}$. We fitted the experimental PNR data to model curves using exact solutions of the Schrödinger equation (for details, see Sec. V in Ref. [37]). We were able to reproduce the experimental curves with a model based on 12 identical pairs with $d_F = 1.7$ nm and $d_S = 25.0$ nm and magnetization of Gd of $4\pi M_{Gd} = 2.5$ kG. Within a measurement error of 10%, this value agrees with 2.7 kG, which can be calculated using the saturation magnetic moment $m_{sat} = 134$ μemu measured by a superconducting quantum interference device (SQUID) magnetometer [inset of Fig. 2(a)] at the same temperature and magnetic field.

Figure 2(b) shows the superconducting phase diagram of sample 1 measured by a standard four-point electrical resistivity technique. This phase diagram allowed us to determine $T_c = 5.5$ K and also the superconducting coherence length $\xi_S = \frac{2}{\pi}\sqrt{\frac{\Phi_0}{2\pi H_{C2\perp}(0)}} = 11.6$ nm. The latter value is in agreement with the previously reported value for Nb films [30].

Figure 3 shows the field and temperature behavior of the spin asymmetry at the first Bragg peak S_1. Above T_c we used the following protocol. First, the sample was magnetized for a short time in the maximum magnetic field $H_{max} = 4.5$ kOe.

FIG. 2. (a) Experimental (dots) neutron reflectivity curves measured on sample 1 at $T = 7$ K and $H = 4.5$ kOe. Solid lines show model curves. Inset: Magnetic hysteresis loops measured at $T = 7$ K by a SQUID magnetometer. (b) Temperature dependencies of the upper critical field measured with external field applied parallel (black) and normal (red) to the surface.
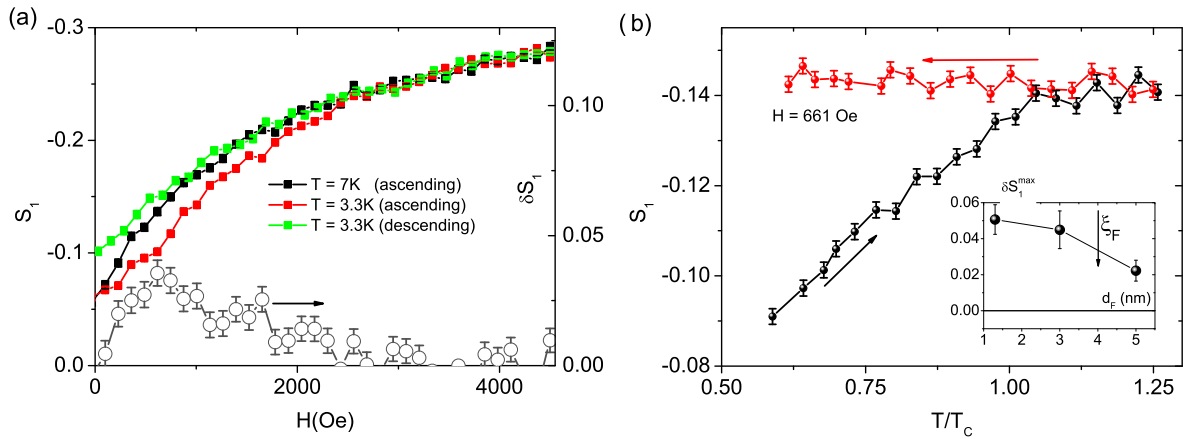
FIG. 3. (a) Magnetic-field-dependent spin asymmetry at the first Bragg peak S_1 measured above T_c (black) and below T_c (red and green). The black and red curves were measured in ascending magnetic field from zero to $H = 4.5$ kOe. The green curve was measured in descending field from saturation to zero. The sample was cooled in zero field below $T_c = 5.5$ K. Open symbols show the difference $\delta S_1 = S_1(7 \text{ K}) - S_1(3 \text{ K})$. (b) Temperature dependence of S_1 measured in the magnetic field $H = 661$ Oe where the maximum of δS_1 was observed. The black curve was measured by increasing the temperature after zero-field cooling (ZFC) and after this the red curve was measured with decreasing temperature. The inset shows the $\delta S_1^{\text{max}}(d_F)$ dependence.

Then the field was released to zero and $S_1(H)$ was measured for ascending magnetic field from 5 Oe to H_{max} [black curve in Fig. 3(a)]. Then the field was released to zero and the sample was cooled down to $T = 3.3$ K in zero magnetic field. After this we repeated $S_1(H)$ by first raising the magnetic field from 5 Oe to H_{max} [red curve in Fig. 3(a)] and then lowering it to $H = 5$ Oe [green curve in Fig. 3(a)]. The $S_1(H)$ curve above T_c repeats qualitatively the behavior of the upper branch of the macroscopic magnetic moment [inset in Fig. 2(a)]: The $S_1(H)$ curve grows from remanence to $H \sim 2$ kOe and then approaches saturation. The corresponding curve below T_c is somewhat suppressed in the range of fields between remanence and saturation. The suppression is maximal around $H \approx 700$ Oe. The descending curve in turn is different at small fields close to zero. In order to check whether this difference is related to the superconducting state, we measured the temperature dependence $S_1(T)$ using the following protocol. Above T_c the sample was magnetized to saturation for a short time and then the field was released to zero and the sample was cooled down to 3.3 K in zero field. Then a field of $H = 661$ Oe was applied and $S_1(T)$ was measured by first heating the sample to $T = 7$ K [black curve in Fig. 3(b)] and then cooling it back in the same field to $T = 3.3$ K. One can see that the amplitude of S_1 is indeed suppressed below T_c if the sample is cooled in zero field. We have conducted similar measurements for the other two samples and observed that the magnitude of the suppression is inversely proportional to d_F [see the inset in Fig. 3(b)]. For sample 3 with $d_F = 1.25\xi_F$ the effect is small but nonvanishing.

We have thus observed a suppression of the spin asymmetry of the first Bragg peak below T_c after zero-field cooling. The effect takes place in an intermediate range of magnetic fields between remanence and saturation. However, we did not observe any additional Bragg peaks below T_c at these magnetic fields. Thus AF alignment or any other modification of the magnetic period can be excluded in our structure. Moreover, in our previous study of Nb(25 nm)/Gd(d_F)/Nb(25 nm) trilayers we did not observe

any statistically significant change of the spin asymmetry below T_c [30]. All these observations point to an electrodynamical origin of the effect. Indeed, for $d_F \sim \xi_F$ two adjacent S layers are expected to be coupled by the proximity effect. This means that the whole sample is a superconductor with thickness $D_S = 12D \approx 300$ nm which is larger than the magnetic screening length $\lambda_{\text{Nb}} \sim 120$ nm in niobium films [38–40]. Such a thick superconductor is able to expel a certain amount of the external field. As a consequence, the central Gd layers feel less of the magnetic field than applied outside and hence their response is smaller. If the sample is cooled in a magnetic field, then magnetic flux is trapped around the Gd layers and the effect is smaller or not seen at all. This model also explains the existence of the effect in the intermediate range of magnetic fields where the derivative $dM/dH \neq 0$. Moreover, the same mechanism explains why we did not see the effect in Nb(25 nm)/Gd/Nb(25 nm) trilayers—the total thickness of the superconductor $D_S = 50$ nm is not enough to expel a significant amount of magnetic flux.

In order to qualitatively describe the suppression of the spin asymmetry we have fitted the neutron data measured on sample 1 above and below T_c in a magnetic field $H = 0.8$ kOe [Figs. 4(a) and 4(b)]. Above T_c we used a model with 12 identical Gd layers. The best fit was obtained for $4\pi M_{\text{Gd}} = 1.4$ kG. To fit the data below T_c we used the following procedure. For the given value of λ we calculated the value of the local magnetic field $H(z)$ at the position of every Gd layer using the well-known expression for the Meissner effect in a superconducting film of thickness D_S and applied magnetic field H_0: $H(z) = H_0 \cosh(z/\lambda)/\cosh(D_S/2\lambda)$. The magnetic response of every Gd layer was then recalculated using this value of $H(z)$ under the assumption that all Gd layers follow the $M(H)$ dependence depicted in the inset to Fig. 2(a). Then, model reflectivity curves for this magnetic configuration were calculated and compared to the experimental curves using the standard goodness-of-fit parameter χ^2. Results of this treatment are shown in Fig. 4, and the best agreement is obtained for $\lambda = 180 \pm 10$ nm [Fig. 4(d)]. This value is considerably
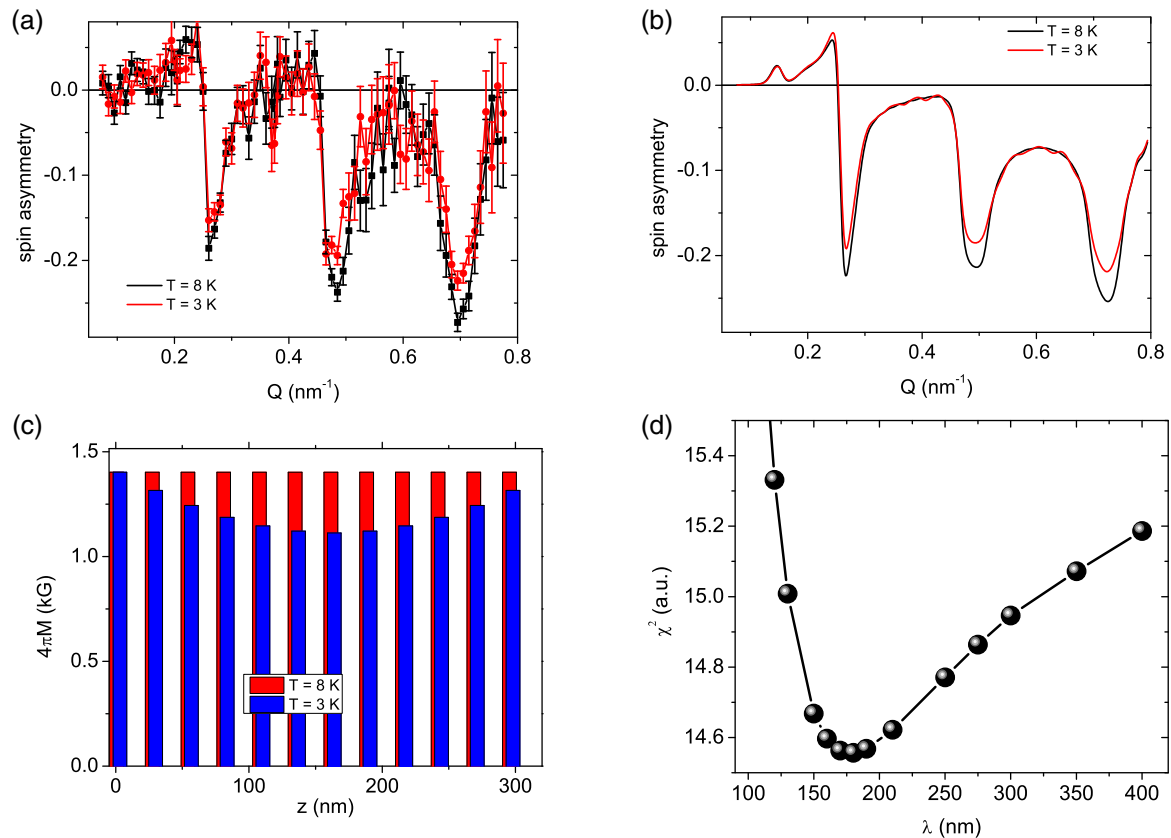
FIG. 4. Experimental spin asymmetry measured on sample 1 above and below T_c. (b) The best-fit model spin asymmetries for the magnetization depth profiles depicted in (c). (d) Dependence of the goodness of fit vs magnetic field penetration depth.

larger than $\lambda \sim 100$ nm for a pure Nb film of similar thickness, which is typical for proximity-coupled multilayers [41–43].

We have thus shown that owing to the proximity effect the entire Gd/Nb superlattice behaves as a uniform thick (magnetic) superconductor. As a thick superconductor it is able to screen the applied magnetic field, thus suppressing the ferromagnetic response of the inner Gd layers. This effect is to some extent similar to the cryptoferromagnetism predicted in Refs. [13–15]. In analogy to CFM, it leads to a transition from homogeneous magnetic order above T_c to inhomogeneous order (along z in our case) below T_c, and hence to a suppression of the averaged magnetic moment. Similar to CFM, the effect takes place for a weakened ferromagnet ($d_F < \xi_F$) and strengthened superconductor ($D_S > \lambda$). Our investigation shows that electromagnetic effects may play a significant role in S/F systems and should be taken into account when considering proximity effects in S/F systems. Note that recent theoretical work came to a related conclusion [44]. Our results demonstrate the potential of elemental S/F multilayers as simple model systems for ferromagnetic superconductors.

[1] A. I. Buzdin, Rev. Mod. Phys. **77**, 935 (2005).

[2] A. A. Golubov, M. Y. Kupriyanov, and E. Il'ichev, Rev. Mod. Phys. **76**, 411 (2004).

[3] F. S. Bergeret, A. F. Volkov, and K. B. Efetov, Rev. Mod. Phys. **77**, 1321 (2005).

[4] M. Eschrig, Phys. Today **64**(1), 43 (2011).

[5] A. Sidorenko, Low Temp. Phys. **43**, 766 (2017).

[6] J. Stahn, J. Chakhalian, C. Niedermayer, J. Hoppler, T. Gutberlet, J. Voigt, F. Treubel, H.-U. Habermeier, G. Cristiani, B. Keimer, and C. Bernhard, Phys. Rev. B **71**, 140509(R) (2005).

[7] J. Chakhalian, J. W. Freeland, G. Srajer, J. Strempfer, G. Khaliullin, J. C. Cezar, T. Charlton, R. Dalgliesh, C. Bernhard,

G. Cristiani, H.-U. Habermeier, and B. Keimer, Nat. Phys. **2**, 244 (2006).

[8] J. Hoppler, J. Stahn, C. Niedermayer, V. K. Malik, H. Bouyanfif, A. J. Drew, M. Rossle, A. Buzdin, G. Cristiani, H.-U. Habermeier, B. Keimer, and C. Bernhard, Nat. Mater. **8**, 315 (2009).

[9] D. K. Satapathy, M. A. Uribe-Laverde, I. Marozau, V. K. Malik, S. Das, T. Wagner, C. Marcelot, J. Stahn, S. Brück, A. Rühm, S. Macke, T. Tietze, E. Goering, A. Frañó, J. H. Kim, M. Wu, E. Benckiser, B. Keimer, A. Devishvili, B. P. Toperverg, M. Merz, P. Nagel, S. Schuppler, and C. Bernhard, Phys. Rev. Lett. **108**, 197201 (2012).

[10] D. Aoki, A. Huxley, E. Ressouche, D. Braithwaite, J. Flouquet, J.-P. Brison, E. Lhotel, and C. Paulsen, Nature (London) **413**, 613 (2001).

[11] C. Pfleiderer, M. Uhlarz, S. Hayden, R. Vollmer, H. v. Löhneysen, N. Bernhoeft, and G. Lonzarich, Nature (London) **412**, 58 (2001).

[12] V. P. Mineev, Phys. Usp. **60**, 121 (2017).

[13] P. W. Anderson and H. Suhl, Phys. Rev. **116**, 898 (1959).

[14] A. I. Buzdin and L. Bulaevskii, JETP **67**, 576 (1988).

[15] F. S. Bergeret, K. B. Efetov, and A. I. Larkin, Phys. Rev. B **62**, 11872 (2000).

[16] Y. Zhu, A. Pal, M. G. Blamire, and Z. H. Barber, Nat. Mater. **16**, 195 (2017).

[17] I. I. Soloviev, N. V. Klenov, S. V. Bakurskiy, M. Y. Kupriyanov, A. L. Gudkov, and A. S. Sidorenko, Beilstein J. Nanotechnol. **8**, 2689 (2017).

[18] A. A. Golubov and M. Y. Kupriyanov, Nat. Mater. **16**, 156 (2017).

[19] M. L. Schneider, C. A. Donnelly, and S. E. Russek, J. Appl. Phys. **124**, 161102 (2018).

[20] I. I. Soloviev, A. E. Schegolev, N. V. Klenov, S. V. Bakurskiy, M. Y. Kupriyanov, M. V. Tereshonok, A. V. Shadrin, V. S. Stolyarov, and A. A. Golubov, J. Appl. Phys. **124**, 152113 (2018).

[21] A. E. Schegolev, N. V. Klenov, I. I. Soloviev, and M. V. Tereshonok, Beilstein J. Nanotechnol. **7**, 1397 (2016).

[22] D. Lenk, V. I. Zdravkov, J.-M. Kehrle, G. Obermeier, A. Ullrich, R. Morari, H.-A. K. von Nidda, C. Müller, M. Y. Kupriyanov, A. S. Sidorenko *et al.*, Beilstein J. Nanotechnol. **7**, 957 (2016).

[23] D. Lenk, R. Morari, V. I. Zdravkov, A. Ullrich, Y. Khaydukov, G. Obermeier, C. Müller, A. S. Sidorenko, H.-A. Krug von Nidda, S. Horn, L. R. Tagirov, and R. Tidecks, Phys. Rev. B **96**, 184521 (2017).

[24] I. P. Nevirkovets and O. A. Mukhanov, Phys. Rev. Appl. **10**, 034013 (2018).

[25] Y. N. Proshin, Y. A. Izyumov, and M. G. Khusainov, Phys. Rev. B **64**, 064522 (2001).

[26] K. Halterman and O. T. Valls, Phys. Rev. B **69**, 014517 (2004).

[27] S. V. Bakurskiy, M. Y. Kupriyanov, A. A. Baranov, A. A. Golubov, N. V. Klenov, and I. I. Soloviev, JETP Lett. **102**, 586 (2015).

[28] I. Nevirkovets and O. A. Mukhanov, Supercond. Sci. Technol. **31**, 03LT01 (2018).

[29] N. Klenov, Yu. Khaydukov, S. Bakurskiy, R. Morari, I. Soloviev, V. Boian, T. Keller, M. Kupriyanov, A. Sidorenko, and B. Keimer, Beilstein J. Nanotechnol. **10**, 833 (2019).

[30] Y. N. Khaydukov, A. S. Vasenko, E. A. Kravtsov, V. V. Progliado, V. D. Zhaketov, A. Csik, Y. V. Nikitenko, A. V. Petrenko, T. Keller, A. A. Golubov, M. Y. Kupriyanov, V. V. Ustinov, V. L. Aksenov, and B. Keimer, Phys. Rev. B **97**, 144511 (2018).

[31] Y. Khaydukov, R. Morari, O. Soltwedel, T. Keller, G. Christiani, G. Logvenov, M. Kupriyanov, A. Sidorenko, and B. Keimer, J. Appl. Phys. **118**, 213905 (2015).

[32] V. Holý and T. Baumbach, Phys. Rev. B **49**, 10668 (1994).

[33] J. Goff, P. Deen, R. Ward, M. Wells, S. Langridge, R. Dalgleish, S. Foster, and S. Gordeev, J. Magn. Magn. Mater. **240**, 592 (2002).

[34] V. Aksenov, K. Jernenkov, Y. Khaidukov, Y. Nikitenko, A. Petrenko, V. Proglyado, G. Andersson, and R. Wäppling, Physica B **356**, 9 (2005).

[35] Y. N. Khaydukov, V. L. Aksenov, Y. V. Nikitenko, K. N. Zhernenkov, B. Nagy, A. Teichert, R. Steitz, A. Rühm, and L. Bottyán, J. Supercond. Novel Magn. **24**, 961 (2011).

[36] Y. N. Khaydukov, B. Nagy, J. H. Kim, T. Keller, A. Rühm, Y. V. Nikitenko, K. N. Zhernenkov, J. Stahn, L. F. Kiss, A. Csik, L. Bottyán, and V. L. Aksenov, JETP Lett. **98**, 107 (2013).

[37] Y. N. Khaydukov, G. A. Ovsyannikov, A. E. Sheyerman, K. Y. Constantinian, L. Mustafa, T. Keller, M. A. Uribe-Laverde, Y. V. Kislinskii, A. V. Shadrin, A. Kalaboukhov, B. Keimer, and D. Winkler, Phys. Rev. B **90**, 035130 (2014).

[38] H. Zhang, J. W. Lynn, C. F. Majkrzak, S. K. Satija, J. H. Kang, and X. D. Wu, Phys. Rev. B **52**, 10395 (1995).

[39] A. I. Gubin, K. S. Il'in, S. A. Vitusevich, M. Siegel, and N. Klein, Phys. Rev. B **72**, 064503 (2005).

[40] Y. Khaydukov, R. Morari, L. Mustafa, J.-H. Kim, T. Keller, S. Belevski, A. Csik, L. Tagirov, G. Logvenov, A. Sidorenko, and B. Keimer, J. Supercond. Novel Magn. **28**, 1143 (2015).

[41] S. M. Yusuf, E. E. Fullerton, R. M. Osgood, and G. P. Felcher, J. Appl. Phys. **83**, 6801 (1998).

[42] A. V. Galaktionov and A. D. Zaikin, Phys. Rev. B **67**, 184518 (2003).

[43] M. Houzet and J. S. Meyer, Phys. Rev. B **80**, 012505 (2009).

[44] S. Mironov, A. Mel'nikov, and A. Buzdin, Appl. Phys. Lett. **113**, 022601 (2018).